Tunable upconverted optical parametric oscillator with intracavity adiabatic sum-frequency generation

Gil Porat,[1,*] Haim Suchowski,[2] Yaron Silberberg,[2] and Ady Arie[1]

[1]*Department of Physical Electronics, Fleischman Faculty of Engineering, Tel Aviv University, Tel Aviv 69978, Israel*
[2]*Department of Physics of Complex System, Weizmann Institute of Science, Rehovot 76100, Israel*
*Corresponding author: gilporat@post.tau.ac.il

We experimentally demonstrate efficient tunable upconversion by cascading optical oscillation and wideband adiabatic sum-frequency generation in a single KTiOPO$_4$ crystal, yielding red light tunable over a 6.2 nm wavelength band. The conversion efficiency of the 1064 nm pump to the red output was up to 4.7%, and with the highest pump power of 1.5 W we obtained 71 mW of average power at 637 nm. © 2010 Optical Society of America

OCIS codes: 190.4223, 190.4970.

Various applications in optics—such as spectroscopy, interferometry, and biosensing—require tunable laser sources over different frequency bands for their execution. Optical parametric oscillators (OPOs) are very efficient devices for generating tunable downconverted light from a fixed-frequency pump. As for the upconversion, several schemes have been suggested [1–9] for the upconversion of the signal of an OPO, thus taking advantage of the wide tunability of this device for the sake of generating a frequency higher than the pump frequency. The upconversion process, be it a second-harmonic generation or a sumfrequency generation (SFG), faces the problem of small acceptance bandwidths, resulting from the higher dispersion of nonlinear crystals at short wavelengths. In order to circumvent this issue, past suggestions required mechanical tuning [2–6], a tunable pump source [7,8], or using high-order processes with low efficiencies [9].

In this Letter we demonstrate a method that overcomes the OPO upconversion small acceptance bandwidth problem and enables one to achieve tunable and efficient upconverted light from a fixed-frequency pump source using a single temperature-tuned crystal. It is applicable for lasers from the cw to the picosecond time regime [10]. For example, it enables one to generate tunable radiation in the visible from near-IR pump sources such as Nd:yttrium aluminum garnet (Nd:YAG) lasers and tunable UV radiation from frequency-doubled Nd:YAG lasers.

In this method, the nonlinear crystal is composed of two cascaded segments as portrayed in Fig. 1: the first segment, of length $L_{periodic}$, is periodically poled to phase match an OPO process, converting the pump wave of frequency ω_p into a signal wave and an idler wave, with frequencies ω_s and ω_i, respectively, satisfying $\omega_p = \omega_s + \omega_i$. The second segment, of length L_{chirp}, is poled with a linear chirp in order to phase-match the SFG of the pump and OPO signal over a large wavelength band of the signal. The sum frequency is $\omega_{SFW} = \omega_p + \omega_s$. Crystals with chirped gratings have been used for various applications, e.g., compression of ultrashort pulses [11] and broadband frequency conversion [12]. Here the chirped segment was constructed to allow an adiabatic SFG as described by Suchowski *et al.* [10,13], which results in an efficient and robust conversion for a broad spectral range. In order to produce an adiabatic passage from the signal to the sum frequency wave (SFW), the phase-mismatch parameter should vary slowly along the propagation axis, from a large negative phase-mismatch value to a large positive one. This purpose is obtained by a linear chirp poling that conforms to the adiabaticity condition

$$\frac{d(\Delta k_{SFG})}{dz} \ll \frac{(\Delta k_{SFG}^2 + \kappa^2)^{3/2}}{\kappa}, \qquad (1)$$

where $\kappa = \{8\pi\omega_s\omega_{SFW}/[(k_s k_{SFW})^{1/2}c^2]\}d_{eff}E_p$ is the nonlinear coupling coefficient; Δk_{SFG} is the SFG process phase-mismatch; ω_s, ω_{SFW}, k_s, and k_{SFW} are the frequencies and propagation constants of the signal and SFW, respectively; c is the velocity of light; d_{eff} is the effective second-order nonlinear coefficient of the crystal; and E_p is the pump amplitude.

The design is based on a 35-mm-long uncoated KTiOPO$_4$ (KTP) crystal whose nonlinear coefficient was modulated by electric field poling (custom-made by Raicol Crystals). For the optimization of the length of each segment of the crystal and the chirp effective periodicity range, a numerical simulation was conducted, applying the split-step Fourier method [14] and taking into account beam diffraction. The optimal values were $L_{periodic} = 27.5$ mm with a period of 35.6 μm for the periodic segment and $L_{chirp} = 7.5$ mm with a periodicity range of $\Lambda(z) = 2\pi/\Delta k(z) = 15.11 - 15.39$ μm for the chirped segment.
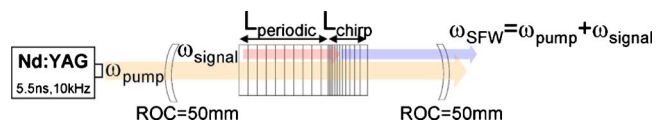

Fig. 1.   (Color online) Setup and crystal structure.

© 2010 Optical Society of America

The crystal was placed in a 55-mm-long linear cavity with two spherical mirrors that have a 50 mm radius of curvature, pumped by a 5.5 ns Nd:YAG laser with a repetition rate of 10 kHz, as described in Fig. 1. The input (output) mirror's pump, signal, idler, and SFW reflectivity were approximately 1% (15%), 68%–99% (83%–87%), 53%–87% (10%–14%), and 82% (54%), respectively. The OPO is single-pass singly resonant for the signal.

The OPO signal and idler wavelengths were designed to tune in the ranges $\lambda_s = 1543 - 1596$ nm and $\lambda_i = 3197 - 3433$ nm by temperature tuning of $30\,°C - 250\,°C$. The corresponding wavelength tuning range of the SFW produced by the SFG process between the $\lambda_p = 1064.5$ nm pump and the signal is $\lambda_{SFW} = 629.92 - 638.58$ nm. The wavelength and temperature dependence of the KTP refractive index were accounted for by the Sellmeier equations of [15,16], yielding phase-mismatch ranges of $\Delta k_{OPO} = 0.1764 - 0.1765$ μm^{-1} and $\Delta k_{SFG} = 0.4136 - 0.4143$ μm^{-1} for the OPO and SFG processes, respectively.

Even for a highly depleted and absorbed pump, with a remaining peak intensity of 50 MW/cm² in the chirped segment, simulation predicts 55%–80% single-pass signal-to-SFW conversion efficiency over the entire tuning range. This simulation follows previous works on adiabatic SFG [10,13], assuming plane waves, no pump depletion by the SFG process, and a lossless medium. Its results can be seen in Fig. 2. Using these experimental parameters, the ratio between the left- and right-hand sides of Eq. (1) is $0.0513 \ll 1$, assuring that the adiabaticity criteria hold.

Two experiments were performed with this crystal. In the first experiment, we studied the tuning properties of the device. The crystal was pumped with a constant average power of 1 W, while the temperature was tuned from $30\,°C$ to $250\,°C$. At each temperature the SFW wavelength and power were measured.

The results of the tuning experiment are displayed in Fig. 3, showing the measured SFW power versus its wavelength, together with simulation results for the same configuration. The SFW average power increases from 27.5 mW at $\lambda_{SFW} = 630.9$ nm to 38.9 mW at $\lambda_{SFW} = 635.3$ nm, and then decreases to 35.1 mW at $\lambda_{SFW} = 637.1$ nm. Therefore the pump-to-SFW conversion efficiency is 2.7%–3.9% over the entire tuning range of the OPO, yielding tunable red light over a 6.22 nm wavelength band, thus demonstrating the robustness of our scheme. For comparison, if a periodic poling pattern with a period of $\Lambda = 15.14$ μm were used throughout the length of $L = 7.5$ mm, our simulation predicts a 2.9 nm FWHM tuning bandwidth around 636.6 nm for the SFW, i.e., 2.1 times less than what was measured with the chirped grating. This would have yielded a low or practically negligible SFG efficiency over most of the OPO tuning range.

The wavelength dependence of the SFW output power is explained using the numerical simulation [14], in which the spectral dependence of the OPO mirrors has also been explicitly introduced. As the SFW wavelength increases toward 636 nm, the OPO idler wavelength gets shorter. Consequently, the idler experiences lower absorption in the KTP crystal [17] and lower overall mirror transmission losses. At the same time, the signal losses are nearly constant, resulting in an increase in the overall parametric gain. This improves the OPO process efficiency, and thus the pump-to-SFW conversion efficiency, and constitutes the reason for the increase in SFW power with wavelength of up to 635.3 nm. For longer SFW wavelengths, idler absorption continues to fall. However, the overall mirror transmission losses for both the idler and signal increase at a greater rate, resulting in an overall lower parametric gain. The OPO process efficiency is thus reduced, yielding a decrease in the pump-to-SFG conversion efficiency. The ~1.5 times lower experimental output power, as compared to the simulation, is attributed to imperfect poling and in-
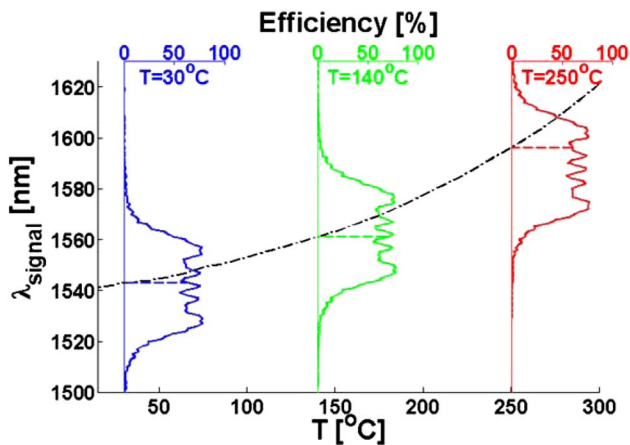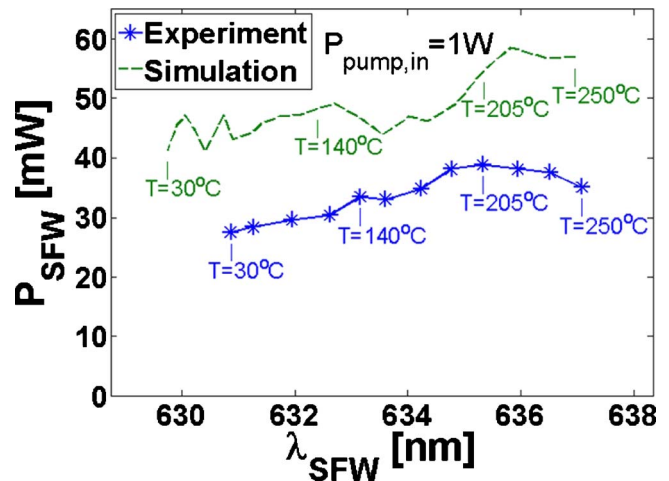

Fig. 2. (Color online) OPO signal tuning (dashed-dotted black) with temperature and adiabatic SFG single-pass signal-to-SFW conversion efficiency (solid blue, green, and red) for peak pump intensity of 50 MW/cm² in the chirped segment, for various crystal temperatures.

Fig. 3. (Color online) Experimental and simulated SFW average output powers when the crystal temperature is tuned from $30\,°C$ to $250\,°C$. The 0–1.2 nm wavelength difference results from greater Sellmeier inaccuracy for the shorter wavelengths.

accuracies in the transmission spectra of the crystal and the mirrors.

We now turn to the second experiment, which studied the conversion efficiency dependence on the pump power. The crystal was kept at a temperature of 250°C, corresponding to λ_{SFW}=637.1 nm, and the input pump power was gradually increased. For each value of the input pump power, the average output powers of the pump, signal, idler, and SFW were measured. This experiment shows how both the OPO and SFG process efficiencies scale with the input pump power.

The resulting average output powers of the signal, idler, and SFW versus the average input pump power are depicted in Fig. 4(a). The SFW power scales quickly with the input pump power, reaching 4.7% pump-to-SFW conversion efficiency at P_{pump}=1.5 W. The corresponding output pump power and pump depletion are presented in Fig. 4(b). The pump depletion was estimated by considering subthreshold pump transmission. The increase in the efficiency with the input pump power is evident in the limiting effect apparent in the output pump power, resulting from increasingly greater depletion of the pump. The high OPO threshold of ~600 mW results from linear losses and nonlinear conversion losses along the chirped segment. Note that the output mirror transmission at the SFW wavelength band is ~46%, indicating an intracavity pump-to-SFW conversion efficiency of up to 10%. Further improvement can be achieved by adding an antireflection coating to the crystal.

Our device exhibits important characteristics like robustness to pump power variations [13], wavelength tunability, and high efficiency. Its performance can be further improved by increasing the temperature tuning range of the OPO signal. This can be achieved by using signal wavelengths closer to degeneracy. For the same temperature tuning range of

30°C−250°C, it can be increased from ~40 nm in the current design to 278 nm by poling the periodic segment of the KTP crystal with a 37.7 μm period. Another method is to use nonlinear crystals that have higher thermal dispersion. For example, tuning magnesium doped lithium niobate from 30°C to 250°C will yield a 392 nm tuning range for the OPO signal, using a 31.2 μm period.

To conclude, we have shown experimentally for the first time (to our knowledge) an efficient temperature-tuned upconverter realized in a single crystal and pumped by a fixed-wavelength laser. Tunable pump upconversion into a wavelength range of 6.22 nm in the red wavelength band with efficiencies of up to 4.7% has been obtained. This scheme has the advantages of simplicity, compactness, and robustness over previous configurations [2–9], while maintaining a high conversion efficiency and a wide tuning range.
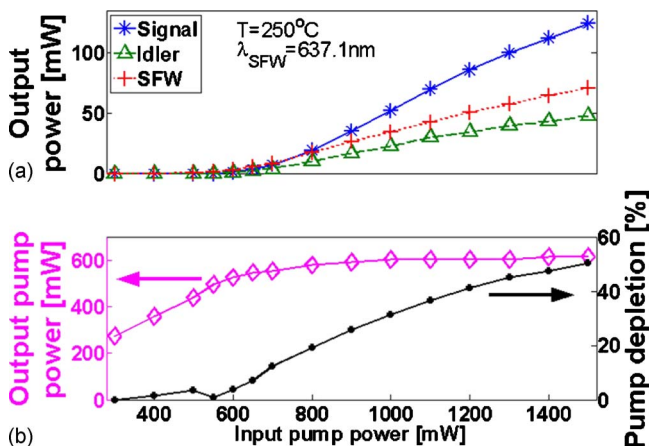
Fig. 4. (Color online) (a) Signal, idler, and SFW average output power versus average input pump power. (b) Average output pump power and pump depletion.

References

1. W. R. Bosenberg, J. I. Alexander, L. E. Myers, and R. W. Wallace, Opt. Lett. **23**, 207 (1998).
2. A. Fix and G. Ehret, Appl. Phys. B **67**, 331 (1998).
3. A. Fix, M. Wirth, A. Meister, G. Ehret, M. Pesch, and D. Weidauer, Appl. Phys. B **75**, 153 (2002).
4. M. Ghotbi, A. Esteban-Martin, and M. Ebrahim-Zadeh, Opt. Lett. **33**, 345 (2008).
5. G. K. Samanta and M. Ebrahim-Zadeh, Opt. Lett. **33**, 1228 (2008).
6. P. Peuser, W. Platz, A. Fix, G. Ehret, A. Meister, M. Haag, and P. Zolichowski, Appl. Opt. **48**, 3839 (2009).
7. S. D. Pan, Y. Yuan, L. N. Zhao, X. J. Lv, and S. N. Zhu, Opt. Express **16**, 18616 (2008).
8. P. Xu, K. Li, G. Zhao, S. Zhu, Y. Du, S. Ji, Y. Zhu, and N. Ming, Opt. Lett. **29**, 95 (2004).
9. S. Tu, A. H. Kung, S. Kurimura, and T. Ikegami, Appl. Opt. **47**, 5762 (2008).
10. H. Suchowski, D. Oron, A. Arie, and Y. Silberberg, Phys. Rev. A **78**, 063821 (2008).
11. A. Galvanauskas, D. Harter, M. A. Arbore, M. H. Chou, and M. M. Fejer, Opt. Lett. **23**, 1695 (1998).
12. A. A. Lagatsky, C. T. A. Brown, W. Sibbett, S. J. Holmgren, C. Canalias, V. Pasiskevicius, F. Laurell, and E. U. Rafailov, Opt. Express **15**, 1155 (2007).
13. H. Suchowski, V. Prabhudesai, D. Oron, A. Arie, and Y. Silberberg, Opt. Express **17**, 12731 (2009).
14. A. V. Smith and R. J. Gehr, J. Opt. Soc. Am. B **16**, 609 (1999).
15. K. Fradkin, A. Arie, A. Skliar, and G. Rosenman, Appl. Phys. Lett. **74**, 914 (1999).
16. S. Emanueli and A. Arie, Appl. Opt. **42**, 6661 (2003).
17. G. Hansson, H. Karlsson, S. Wang, and F. Laurell, Appl. Opt. **39**, 5058 (2000).